Interpretable Graph Attention for Autism Brain Networks

Teo Benarous
teo.benarous@mail.mcgill.ca
McGill University
Montreal, Quebec, Canada

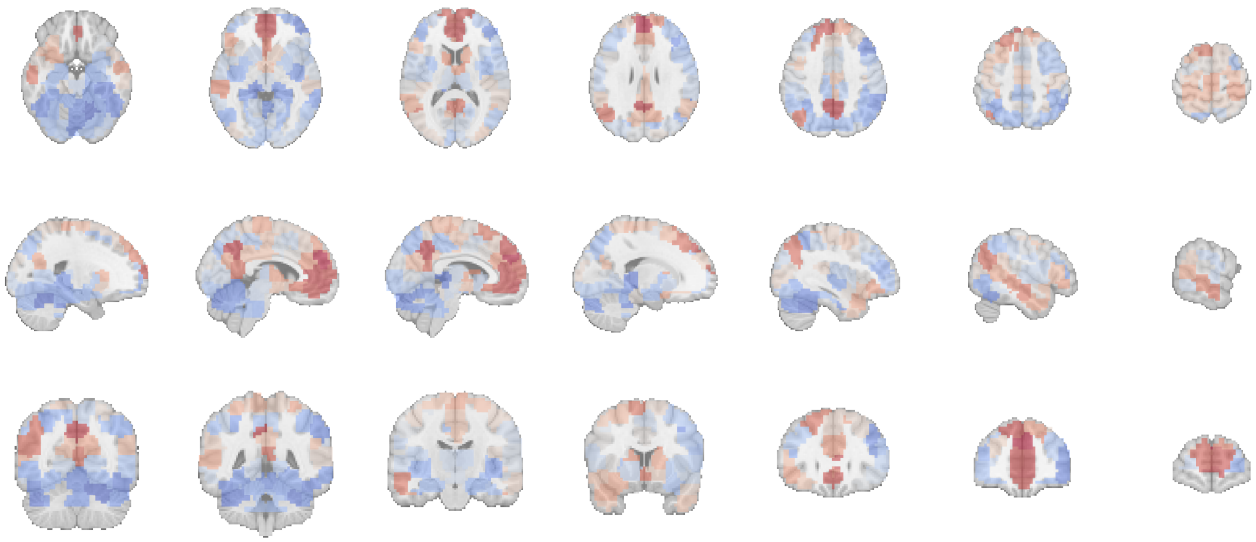

Figure 1: Influential ROIs in ASD Classification.

Abstract

Autism Spectrum Disorder (ASD) presents heterogeneous manifestations, complicating imaging-based classification. This study presents a case study on ASD classification using graph neural networks (GNNs) applied to rs-fMRI data from the Autism Brain Imaging Data Exchange. Connectomes were constructed using partial correlations for edge connectivity, with Pearson correlations and region-specific neural dynamics for node features. A graph attention model with hierarchical pooling was employed, reflecting the brain's multi-scale functional architecture. While classification accuracy aligns with prior GNN-based approaches, the primary focus of this work is interpretability. Using GNNExplainer, we identify influential regions of interest, including the precuneus and inferior parietal lobule, consistent with established ASD literature.

Keywords

Graph Neural Networks, Autism Spectrum Disorder, Brain Connectomics, Interpretability

COMP 511 Final Projects, Montreal, QC, CA

1 Introduction and Motivation

Autism Spectrum Disorder (ASD) is a complex neurodevelopmental condition characterized by difficulties in social communication, restricted interests, and repetitive behaviors. Given ASD's heterogeneous manifestations, identifying robust biomarkers remains a significant challenge in clinical neuroscience. Resting-state functional magnetic resonance imaging (rs-fMRI) [1] offers a window into intrinsic brain activity by measuring spontaneous fluctuations in the blood-oxygen-level-dependent (BOLD) signal without task-driven stimuli. These fluctuations reflect neural dynamics and form the basis for functional connectivity analysis.

Statistical dependencies between regional BOLD time series typically define functional connectivity. By parcellating the brain into discrete regions of interest (ROIs), one can compute mean time series within each region and use these to infer connectivity patterns. These patterns can be represented as graphs, where nodes correspond to ROIs and edges encode functional relationships. In this form, the brain's dynamics become legible to models that operate not just on data but on the structure itself.

We propose an interpretable graph neural network (GNN) framework for ASD classification using rs-fMRI data from the Autism Brain Imaging Data Exchange (ABIDE) [6]. Our approach integrates two complementary measures of functional connectivity: Pearson correlation and partial correlation. While Pearson correlation captures global co-activation patterns, partial correlation isolates direct statistical dependencies by conditioning out the influence of other

regions. We leverage this complementarity by using partial correlations to define the edge connectivity and Pearson correlations to define node features. This design is inspired by recent work in multi-view and multi-graph neuroimaging, which demonstrates that integrating distinct connectivity views enhances discriminative power and interpretability [16].

Incorporating attention mechanisms and hierarchical pooling within the GNN allows us to identify salient substructures in the brain graph that contribute to classification. Post hoc explanation tools, such as GNNExplainer [18], highlight influential nodes and edges, offering neuroscientific insight into model predictions. Through this pipeline, we aim to build an interpretable classifier for ASD based on resting-state brain connectivity.

2 Related Work

Graph Neural Networks for Brain Connectomics. Brain networks naturally lend themselves to graph-based representations, where ROIs map to nodes and functional or structural connections map to edges. Conventional graph-theoretical metrics (e.g., clustering coefficient, modularity) provided early insights into neurological conditions, yet their hand-engineered nature may miss subtle multi-regional interactions [3, 13]. Graph Convolutional Networks (GCNs) [9] introduced a learnable mechanism for node feature aggregation across the network, improving performance on various classification tasks, including neurological disorders [10].

Attention and Pooling in Graph Neural Networks. Uniform neighborhood aggregation in standard GCN layers can dilute critical edges. Graph Attention Networks (GATs) [17] address this by assigning learnable attention coefficients to each edge, refining the influence of highly relevant connections in the embedding process. Hierarchical pooling approaches like SAGPool [11] and DiffPool [19] further reduce graph complexity by aggregating nodes into representatives, intuitively aligning with the multi-scale organization of functional brain networks. While these pooling approaches have been validated on benchmark datasets, questions remain about their utility and optimal configuration for real-world neuroimaging data, such as multi-site cohorts like ABIDE.

Interpretable Graph Neural Networks in Neuroimaging. Deep learning approaches in healthcare demand explanation: clinicians not only need to see whether a model performs well but also why it outputs a particular decision [14]. GNNExplainer [18] uncovers which subgraph and features drive a GNN's prediction, yielding insights that can guide neuroscientific interpretations and help validate model outputs against established knowledge of ASD-related networks.

3 Problem Definition

Each participant $k \in \{1, \ldots, M\}$ is assigned a binary label $y^{(k)} \in \{0, 1\}$ indicating ASD diagnosis (1) or typical development (0). We represent the brain as a graph $\mathcal{G}^{(k)} = (\mathcal{V}, \mathcal{E}^{(k)})$ constructed from preprocessed rs-fMRI data. The brain is parcellated into N regions of interest (ROIs), giving rise to $|\mathcal{V}| = N$ nodes. Let $\mathbf{T}^{(k)} \in \mathbb{R}^{T \times N}$ denote the matrix of mean time series of each ROI for subject k, where T is the number of timepoints.

To define edge connectivity, we compute the partial correlation matrix $\mathbf{\Pi}^{(k)}$ by inverting the empirical covariance matrix $\Sigma^{(k)}$ of the of the ROIs' time series. The partial correlation between ROI i and j is given by:

$$\pi_{ij}^{(k)} = \frac{\Theta_{ij}^{(k)}}{\sqrt{\Theta_{ii}^{(k)} \Theta_{jj}^{(k)}}} \tag{1}$$

where $\mathbf{\Theta}^{(k)}$ is the precision matrix. To enforce sparsity and reduce noise, we retain only the top 10% of connections based on the absolute partial correlation values to form the adjacency matrix $\mathbf{A}^{(k)} \in [0, 1]^{N \times N}$:

$$\mathbf{A}_{ij}^{(k)} = \begin{cases} \left|\pi_{ij}^{(k)}\right| & \text{if } \left|\pi_{ij}^{(k)}\right| > \tau^{(k)} \\ 0 & \text{otherwise} \end{cases} \tag{2}$$

where $\tau^{(k)}$ is the threshold corresponding to the 90-th percentile of the absolute non-zero partial correlations.

Node features are defined by combining multiple types of ROI-level information. We first consider the Pearson correlation coefficients. To enrich each ROI's representation, we include scalar features derived from neural dynamics. These include: (1) the amplitude of low-frequency fluctuations (fALFF) [21], which quantifies the relative power of spontaneous BOLD signal fluctuations in the 0.01–0.1 Hz band and is associated with regional spontaneous activity; (2) regional homogeneity (ReHo) [20], which measures the similarity of a voxel's time series to those of its immediate neighbors and reflects local synchronization; and (3) the mean BOLD signal amplitude, representing the average signal intensity over time within a region, which may capture baseline regional activity levels. Let $a_i^{(k)}$, $r_i^{(k)}$, and $m_i^{(k)}$ denote the fALFF, ReHo, and mean amplitude for ROI i, respectively. The node feature vector is then given by:

$$\mathbf{x}_i^{(k)} = \left(\rho_{i1}^{(k)}, \rho_{i2}^{(k)}, \ldots, \rho_{iN}^{(k)}, a_i^{(k)}, r_i^{(k)}, m_i^{(k)}\right)^\top \in \mathbb{R}^{N+3} \tag{3}$$

This composite feature vector integrates global co-activation profiles with local region-specific properties, enabling the model to learn network topology and regional functional characteristics.

Additionally, we include graph-level features which capture phenotypic information that may influence neuroimaging patterns but applies uniformly across the entire brain graph for a participant. Specifically, we include four categorical features: acquisition site, sex, eye status at scan, and handedness; and four numerical features: age of the patient, full-scale IQ (FIQ), verbal IQ (VIQ), and performance IQ (PIQ).

The resulting graph, integrating node-level neural dynamics and connectivity information with graph-level phenotypic context, is passed through a multi-layer graph neural network (GNN) architecture composed of Graph Attention Network (GAT) layers and hierarchical pooling modules. A final readout layer combines node embeddings with the phenotypic features, producing a unified graph-level embedding to predict the diagnostic label. Interpretability is facilitated by GNNExplainer, which identifies relevant subgraphs and node features that drive the model's prediction.

4 Dataset Description

The Autism Brain Imaging Data Exchange (ABIDE) [6] is a large multi-site repository containing over one thousand resting-state fMRI scans from individuals with ASD and matched TD controls.

We utilize the ABIDE Preprocessed repository [4] to ensure preprocessing consistency, specifically selecting the CPAC-preprocessed pipeline with bandpass filtering enabled and global signal regression disabled. All fMRI scans are normalized to MNI152 space, a standardized anatomical brain template, and temporally filtered to retain frequencies in the 0.01–0.1 Hz range.

The brain is parcellated using the Craddock 200 (CC200) functional atlas [5], which divides the brain into $N = 200$ spatially coherent ROIs. For each participant, we extract the mean BOLD time series within each ROI, forming the basis for defining our framework's edge connectivity and node features.

5 Methodology

The ABIDE dataset is slightly unbalanced, with more TD than ASD participants (Figure 2.a). The age distribution (Figure 2.b) is centered around adolescence, with both groups spanning a broad developmental range. The number of subjects per site (Figure 2.c) highlights the multi-site nature of ABIDE and variability in per-site sample sizes.

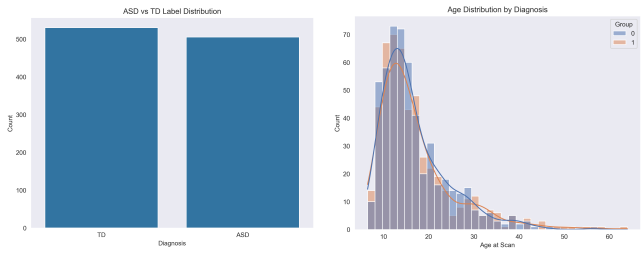

(a) (b)

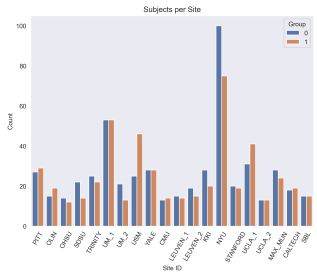

(c)

Figure 2: Distribution of patients. (a) Per diagnosis. (b) Per age. (c) Per site.

Figure 3 shows the Craddock 200 atlas overlaid on a brain template, illustrating the spatial distribution of ROIs used in all subsequent analyses. The overall model pipeline is illustrated in Figure 4.

We present visualizations from a single subject (Subject 0) to further illustrate our graph construction framework. Node features are derived from Pearson correlation coefficients and three ROI-level metrics: fALFF, ReHo, and mean BOLD amplitude. The distributions of fALFF and ReHo across ROIs are shown in Figures 5.a and 5.b, respectively. Figure 6 displays five time series from randomly selected ROIs.

Functional connectivity is quantified using both Pearson and partial correlation. Figure 8 shows the corresponding matrices and

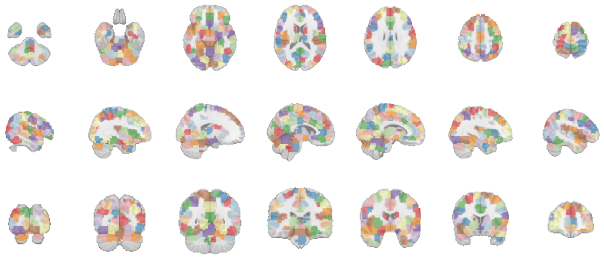

Figure 3: Slices of the Craddock 200 atlas. (Top) Along the x-axis. (Middle) Along the y-axis. (Bottom) Along the z-axis.

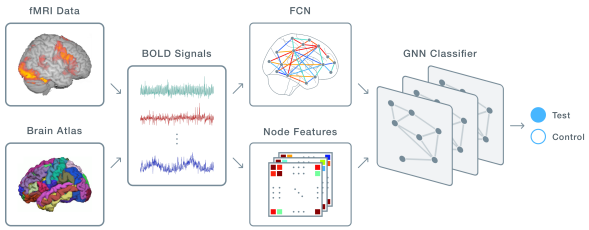

Figure 4: Model pipeline. Adapted from [15].

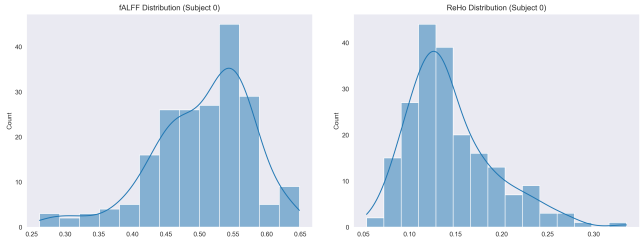

(a) (b)

Figure 5: Distribution of node features for Subject 0. (a) fALFF Distribution. (b) ReHo Distribution.

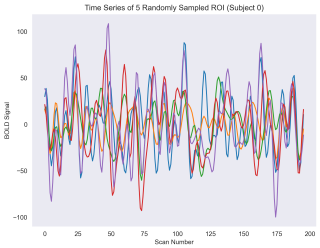

Figure 6: Time series of five randomly sampled ROIs for Subject 0.

the binarized adjacency matrix formed by thresholding the partial correlations at the 90th percentile. The final subject-specific graph is visualized in Figure 9, with nodes positioned anatomically and edges representing retained partial correlations. This example highlights the structure input graphs used for model training.

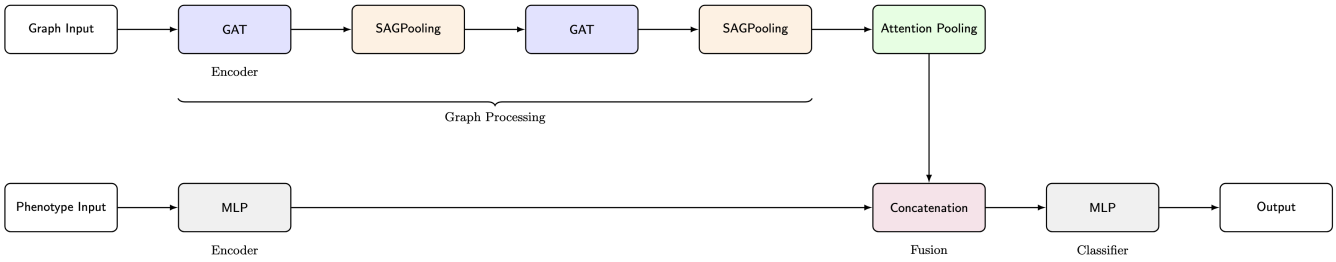

Figure 7: Model Architecture.

The model of interest, which combines attention layers and hierarchical pooling, is illustrated in Figure 7.

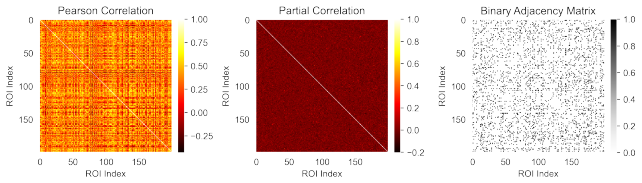

Figure 8: Functional Connectivity Matrices for Subject 0.

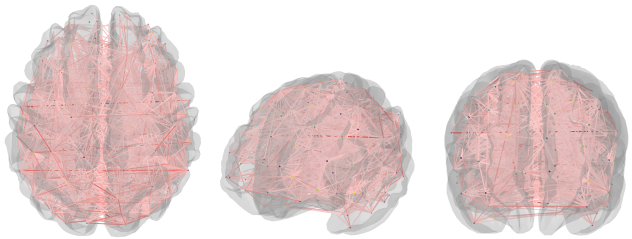

(a) **(b)** **(c)**

Figure 9: Connectome of Subject 0. The redness of the links represent partial correlations. (a) Top. (b) Front/Left. (c) Front.

6 Experimental Setup

Baseline model. We implement a two-layer Graph Convolutional Network (GCN) using PyTorch Geometric [7]. Each layer has 64 hidden neurons with ReLU activations, followed by global mean pooling and a linear layer for binary classification. Dropout regularization, with probability $p = 0.3$, is applied after the first GCN layer.

Model of interest. We implement a graph neural network based on GATv2 layers [2]–an improved variant of GAT that replaces its static attention mechanism with dynamic attention, allowing attention scores to be conditioned on both source and target nodes and thereby increasing expressiveness–and incorporate hierarchical pooling. The architecture consists of two graph attention layers. The first employs 4 attention heads with output features averaged across heads (rather than concatenated), yielding a 64-dimensional node embedding. The second uses a single-head attention layer, maintaining the same dimensionality. Each graph convolution is followed by an ELU activation and dropout regularization with probability $p = 0.3$. To progressively reduce graph resolution while preserving informative substructures, we apply SAGPooling after each convolution, with pooling ratios of 0.85 and 0.65, respectively. To obtain a graph-level representation, we use a learnable attention-based aggregation mechanism: a two-layer multilayer perceptron (MLP) computes scalar attention weights over node embeddings, producing a weighted sum of node features.

Phenotypic features. For both models, the 8-dimensional phenotypic features are projected into the latent space via a linear transformation followed by a ReLU activation. The graph and phenotype embeddings are concatenated and passed through a final two-layer MLP with dropout regularization for binary classification.

Model training and evaluation. The two models are trained using the AdamW optimizer [12]–an optimization algorithm that modifies the implementation of weight decay in Adam [8] by decoupling weight decay from the gradient update–, with a learning rate of 0.001 and a weight decay of 0.0005, and binary cross-entropy loss with logits that account for class imbalance through a positive class weight. Model performance is evaluated using two approaches: (1) an 80/20 random train/test split and (2) leave-one-site-out (LOSO) cross-validation to assess generalization across sites. Performance metrics include Accuracy, Precision, Recall, F1 Score, and ROC-AUC.

7 Results

To assess structural consistency across the cohort, we compute an edge frequency matrix indicating how often each edge appears in the binarized graphs across all subjects. As shown in Figure 10, most edges occur infrequently, with a small subset of pairs of ROIs appearing consistently across individuals.

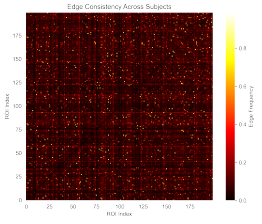

Figure 10: Edge connectivity across subjects.

As a baseline, we implement a two-layer GCN using global mean pooling and dropout regularization. When evaluated with an 80/20 random split repeated over five runs, the model achieves an average accuracy of about 61%. In contrast, the proposed model, incorporating graph attention mechanisms and hierarchical pooling reached an average accuracy of 68.2%. Classification metrics are reported in Table 1. Under a leave-one-site-out (LOSO) evaluation, performance slightly varies across sites (Table 2, Figure 11), e.g., accuracy varies by about 5% across sites for the GAT and 7% for the GCN (standard deviations). Notably, the GAT consistently outperforms the GCN on nearly all sites, often by a substantial margin. For instance, at OHSU the GAT achieves over 25 percentage points higher accuracy than the GCN. This suggests that the GAT generalizes more effectively to out-of-distribution data, while the GCN appears to overfit residual noise linked to site-specific variability, despite extensive preprocessing of the time series.

Table 1: Classification metrics, averaged over 5 runs.

Metric	GCN	GAT
Accuracy	0.610 ± 0.041	0.682 ± 0.020
Precision	0.588 ± 0.041	0.680 ± 0.011
Recall	0.755 ± 0.098	0.680 ± 0.074
F1 Score	0.656 ± 0.033	0.678 ± 0.035
ROC-AUC	0.675 ± 0.0165	0.714 ± 0.022

Table 2: LOSO Classification Metrics.

Site	Accuracy		Precision		Recall		F1 Score		ROC-AUC	
	GCN	GAT	GCN	GAT	GCN	GAT	GCN	GAT	GCN	GAT
CALTECH	0.51	0.68	0.52	0.64	0.84	0.84	0.64	0.73	0.65	0.70
CMU	0.70	0.70	0.71	0.80	0.71	0.57	0.71	0.67	0.74	0.78
KKI	0.58	0.77	0.50	0.76	0.90	0.65	0.64	0.70	0.75	0.71
LEUVEN_1	0.66	0.76	0.75	0.89	0.43	0.57	0.55	0.70	0.72	0.81
LEUVEN_2	0.65	0.79	0.71	0.90	0.33	0.60	0.45	0.72	0.79	0.84
MAX_MUN	0.62	0.65	0.57	0.67	0.71	0.50	0.63	0.57	0.59	0.65
NYU	0.68	0.71	0.60	0.72	0.76	0.55	0.67	0.62	0.72	0.77
OHSU	0.54	0.81	0.50	0.82	0.75	0.75	0.60	0.78	0.64	0.79
OLIN	0.62	0.68	0.62	0.79	0.84	0.58	0.71	0.67	0.60	0.68
PITT	0.57	0.71	0.61	0.78	0.48	0.62	0.54	0.69	0.70	0.75
SBL	0.50	0.70	0.50	0.80	0.87	0.53	0.63	0.64	0.58	0.70
SDSU	0.72	0.78	0.62	0.71	0.71	0.71	0.67	0.71	0.75	0.75
STANFORD	0.54	0.67	0.51	0.62	0.95	0.84	0.67	0.71	0.70	0.71
TRINITY	0.55	0.70	0.52	0.62	0.77	0.91	0.62	0.74	0.65	0.69
UCLA_1	0.67	0.74	0.81	0.78	0.54	0.76	0.65	0.77	0.72	0.75
UCLA_2	0.73	0.81	0.69	0.79	0.85	0.85	0.76	0.81	0.78	0.84
UM_1	0.61	0.67	0.57	0.61	0.87	0.94	0.69	0.74	0.72	0.61
UM_2	0.59	0.65	0.47	0.57	0.69	0.31	0.56	0.40	0.71	0.56
USM	0.65	0.82	0.92	0.85	0.50	0.87	0.65	0.86	0.79	0.88
YALE	0.59	0.71	0.56	0.75	0.79	0.64	0.66	0.69	0.70	0.73

The regions identified as most influential for distinguishing individuals with ASD from TD controls closely align with functional domains consistently implicated in autism research, validating established findings and reinforcing the plausibility and interpretability of our model. The angular gyri (bilaterally), along with the right superior frontal and middle orbitofrontal cortices, emerged as top predictors for ASD. These areas are involved in social cognition, attention control, and reward processing–domains frequently altered in ASD. The left precuneus, another high-importance region, plays a central role in self-referential thinking and default mode network activity, which are often disrupted in autism. In contrast,

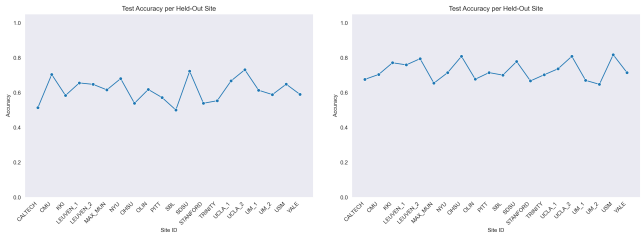

(a) (b)

Figure 11: Accuracy per Held-Out Site. (a) GCN. (b) GAT.

the most predictive regions for TD individuals included the left superior medial frontal gyrus, left medial orbitofrontal cortex, and right anterior cingulate cortex–regions critical to emotion regulation, executive function, and adaptive control, which are frequently compromised in ASD.

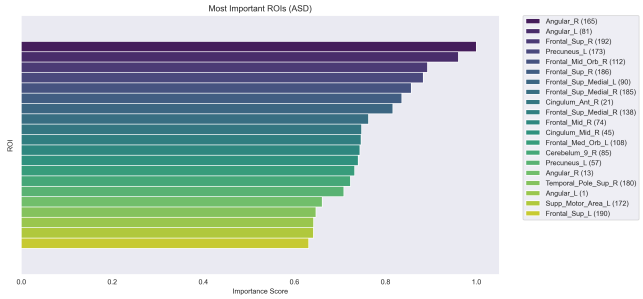

Figure 12: Top 20 ROIs (ASD).

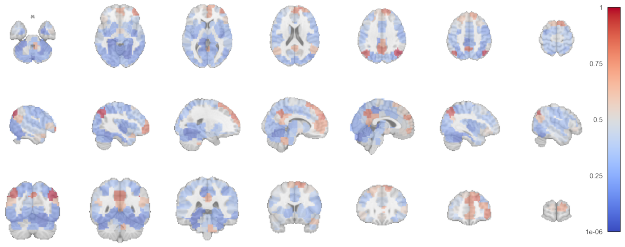

Figure 13: Influential ROIs (ASD).

8 Discussion

Our study demonstrates that a graph neural network (GNN) incorporating attention mechanisms and hierarchical pooling effectively classifies Autism Spectrum Disorder (ASD) from resting-state functional MRI data. The superior performance of the proposed model relative to the baseline Graph Convolutional Network (GCN) underscores the utility of attention-based architectures when paired with hierarchical pooling. This combination allows for capturing multi-scale brain network structures, aligning well with the known hierarchical organization of functional brain connectivity.

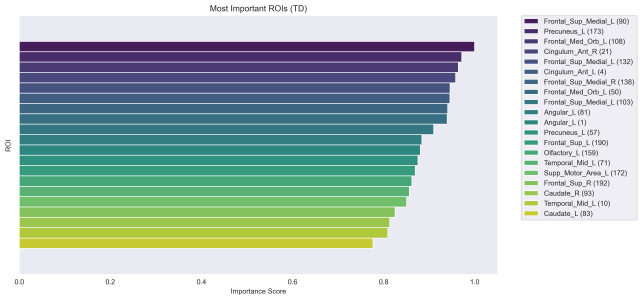

Figure 14: Top 20 ROIs (TD).

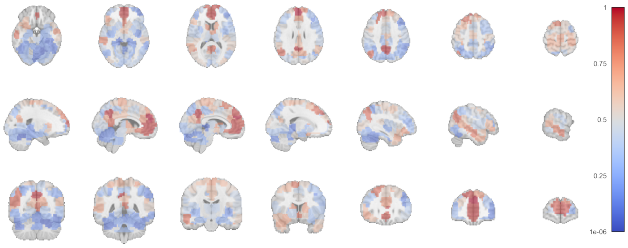

Figure 15: Influential ROIs (TD).

Importantly, the post-hoc interpretability method, GNNExplainer, accurately identified influential regions of interest (ROIs) consistent with established neuroscientific findings. Regions such as the precuneus, supramarginal gyrus, and inferior parietal lobule emerged as predictive for ASD classification, aligning with prior literature highlighting their involvement in social cognition, sensory integration, and self-referential processes. These findings essentially validate the utility of GNNExplainer as an interpretability tool, although recent work has demonstrated that more robust methods are needed.

Although the performance metrics are not particularly high, they are consistent with prior research. For example, BrainGNN, a GCN with ROI-aware message passing, achieved an accuracy of about 65% on this dataset. Modeling each connectome as a temporal network has been shown to yield slightly better performance. State-of-the-art transformer-based methods report accuracy improvements ranging from +5% to +12% above our results.

In summary, our approach demonstrates that GNNExplainer, a GNN-based post-hoc interpretability method, identifies ROIs consistent with prior research in neuroscience and psychology. However, several limitations must be acknowledged. Interpretations from GNNExplainer remain associative and require validation through targeted clinical studies. Additionally, the binary classification framework simplifies the ASD spectrum; future research could extend the analysis to multi-class or dimensional frameworks to more fully capture ASD heterogeneity.

Furthermore, to better handle multi-site data variability and improving generalization, future work could investigate methods such as domain adaptation or transfer learning. [Future work on fusion model; going beyond a simple MLP, but other models, e.g., attention-based ones] [Future work could also explore].

9 Conclusion

We introduced a graph attention network framework successfully classifying ASD from resting-state fMRI data and demonstrated, through GNNExplainer, accurate post-hoc identification of influential brain regions consistent with established neuroscientific literature. Our results highlight the effectiveness of hierarchical pooling and attention mechanisms in GNNs for brain connectomics, achieving competitive accuracy with significant interpretability advantages provided by GNNExplainer. Although transformer-based models achieve higher classification performance, the clear neurobiological interpretability offered through our approach presents an essential advantage for clinical translation and neuroscientific validation. Future research will focus on addressing multi-site generalization challenges and validating interpretability findings through clinical interventions and longitudinal studies.

References

[1] Bharat Biswal, F Zerrin Yetkin, Victor M Haughton, and James S Hyde. 1995. Functional connectivity in the motor cortex of resting human brain using echo-planar MRI. *Magnetic resonance in medicine* 34, 4 (1995), 537–541.

[2] Shaked Brody, Uri Alon, and Eran Yahav. 2021. How attentive are graph attention networks? *arXiv preprint arXiv:2105.14491* (2021).

[3] Ed Bullmore and Olaf Sporns. 2009. Complex brain networks: graph theoretical analysis of structural and functional systems. *Nature reviews neuroscience* 10, 3 (2009), 186–198.

[4] Cameron Craddock, Yassine Benhajali, Carlton Chu, Francois Chouinard, Alan Evans, András Jakab, Budhachandra Singh Khundrakpam, John David Lewis, Qingyang Li, Michael Milham, et al. 2013. The neuro bureau preprocessing initiative: open sharing of preprocessed neuroimaging data and derivatives. *Frontiers in Neuroinformatics* 7, 27 (2013), 5.

[5] R Cameron Craddock, G Andrew James, Paul E Holtzheimer III, Xiaoping P Hu, and Helen S Mayberg. 2012. A whole brain fMRI atlas generated via spatially constrained spectral clustering. *Human brain mapping* 33, 8 (2012), 1914–1928.

[6] Adriana Di Martino, Chao-Gan Yan, Qingyang Li, Erin Denio, Francisco X Castellanos, Kaat Alaerts, Jeffrey S Anderson, Michal Assaf, Susan Y Bookheimer, Mirella Dapretto, et al. 2014. The autism brain imaging data exchange: towards a large-scale evaluation of the intrinsic brain architecture in autism. *Molecular psychiatry* 19, 6 (2014), 659–667.

[7] Matthias Fey and Jan Eric Lenssen. 2019. Fast graph representation learning with PyTorch Geometric. *arXiv preprint arXiv:1903.02428* (2019).

[8] Diederik P Kingma and Jimmy Ba. 2014. Adam: A method for stochastic optimization. *arXiv preprint arXiv:1412.6980* (2014).

[9] Thomas N Kipf and Max Welling. 2016. Semi-supervised classification with graph convolutional networks. *arXiv preprint arXiv:1609.02907* (2016).

[10] Sofia Ira Ktena, Sarah Parisot, Enzo Ferrante, Martin Rajchl, Matthew Lee, Ben Glocker, and Daniel Rueckert. 2017. Distance metric learning using graph convolutional networks: Application to functional brain networks. In *Medical Image Computing and Computer Assisted Intervention- MICCAI 2017: 20th International Conference, Quebec City, QC, Canada, September 11-13, 2017, Proceedings, Part I 20*. Springer, 469–477.

[11] Junhyun Lee, Inyeop Lee, and Jaewoo Kang. 2019. Self-attention graph pooling. In *International conference on machine learning*. pmlr, 3734–3743.

[12] Ilya Loshchilov and Frank Hutter. 2017. Decoupled weight decay regularization. *arXiv preprint arXiv:1711.05101* (2017).

[13] Mikail Rubinov and Olaf Sporns. 2010. Complex network measures of brain connectivity: uses and interpretations. *Neuroimage* 52, 3 (2010), 1059–1069.

[14] Wojciech Samek, Grégoire Montavon, Andrea Vedaldi, Lars Kai Hansen, and Klaus-Robert Müller. 2019. *Explainable AI: interpreting, explaining and visualizing deep learning*. Vol. 11700. Springer Nature.

[15] Jonathan Shobrook and Paul C. Bogdan. 2020. DeepFCN. https://github.com/shobrook/DeepFCN. Created as part of research in the Dolcos Lab at the Beckman Institute for Advanced Science and Technology.

[16] Stephen M Smith, Karla L Miller, Gholamreza Salimi-Khorshidi, Matthew Webster, Christian F Beckmann, Thomas E Nichols, Joseph D Ramsey, and Mark W Woolrich. 2011. Network modelling methods for FMRI. *Neuroimage* 54, 2 (2011), 875–891.

[17] Petar Veličković, Guillem Cucurull, Arantxa Casanova, Adriana Romero, Pietro Lio, and Yoshua Bengio. 2017. Graph attention networks. *arXiv preprint arXiv:1710.10903* (2017).

[18] Zhitao Ying, Dylan Bourgeois, Jiaxuan You, Marinka Zitnik, and Jure Leskovec. 2019. Gnnexplainer: Generating explanations for graph neural networks. *Advances in neural information processing systems* 32 (2019).

[19] Zhitao Ying, Jiaxuan You, Christopher Morris, Xiang Ren, Will Hamilton, and Jure Leskovec. 2018. Hierarchical graph representation learning with differentiable pooling. *Advances in neural information processing systems* 31 (2018).

[20] Yufeng Zang, Tianzi Jiang, Yingli Lu, Yong He, and Lixia Tian. 2004. Regional homogeneity approach to fMRI data analysis. *Neuroimage* 22, 1 (2004), 394–400.

[21] Qi-Hong Zou, Chao-Zhe Zhu, Yihong Yang, Xi-Nian Zuo, Xiang-Yu Long, Qing-Jiu Cao, Yu-Feng Wang, and Yu-Feng Zang. 2008. An improved approach to detection of amplitude of low-frequency fluctuation (ALFF) for resting-state fMRI: fractional ALFF. *Journal of neuroscience methods* 172, 1 (2008), 137–141.